ON MINIMIZING MECHANICAL STRESSES OF THE RAIL WAY WHEELS

H. Moosavi and M. Esfahanian

Department of Mechanical Engineering
Isfahan university of Technology
Isfahan, Iran

(Received: November 18, 1998 - Accepted in Revised Form: July 29, 1999)

Abstract The purpose of this paper is to study the behavior of elastic-plastic stresses under severe drag braking. A railway wheel performs three tasks, aiding in trian movement, supporting the car load, and acting as a brake drum. Finite element computer programs are developed for elasto-plastic stress analysis. An attempt is made here to find an improved fillet profile of the wheel with the intention of minimizing high tensile mechanical stresses. Three new fillet profiles for the wheel are tested. A penalty function is used as a criterion for comparison of stresses between the new designs and the old design. The design with the least penalty is chosen to be the improved one.

Key Words Railway Wheels, Mechanical Stresses, Profile Optimization

»Ì«°B¸Ç« k½kÇ{ q«oÇÙ SdÇÙ nB¤¹ foa nj ð¼ÌwÀÇ-±Ìw¿Á °B´z®Ù nBÌµn »wno¶ ³¸B¸« Ë¼Á ² kµ **²k¼ña**
²k´î ³¶ Án q«oÙ foa ¬Ñ±®î³¶ joñ¦ªî° Ë£Ñ° nB¶ ¥ªdÙ ,nB¤¹ S½oe ³¶ ð ª½ ³´¼©° ³w nB¤¹ foa ð½/k{B¶»«
³®¼´Ç¶ °BÌwÁn nj /SwÁ ²k{ ³¼´Ù ð¼ÌwÀÇ-±Ìw¿Á °B´z®Ù ¥¼¦dÙ °ko¶ j°kd« ¬Bª$Á °oÙ±¼P«B½ °Bµ³«B¯o¶/jnÁj
°ko¶ k½k] ³¦¼µ ¥¼µ°oÇ³w °²k{ y {±½,»ñ¼Bñ« ònq¶»zz½ °B´z®Ù ¬jo½©½ S¼¯B¶, foa ³¦¼µ ¥¼µ°oÇ¬jo½¦
²jB´ÌwÁ ©½k¹ ° k½k] °Bµ¥¼µ°oÇ Ë¼¶ B´z®Ù ³v½B¸« nB¼í« ³ª¼o] é¶BÙ ð ½ pÁ/SwÁ ²k{ ¬±«pÇ° bo¥ nB¤¹ foa
/SwÁ ²k{ JBhÌ¯Á ³®¼´¶ bo¥ ¬Ñ±®î³¶ SwÁnÁj Án ³ª¼o] Ë¼oÌª½ ³½ »¦¼µ°oÇ° ²k{

INTRODUCTION

Since the time- of the first steam engine to the present day the railway system has evolved considerably. The increasing demand for high speed and heavy loads has led to occasional accidents. According to statistics on accidents, compiled by the US Federal Railroad Administration, there has been a yearly average of 324 reportable derailments due to wheel defects and failure which has caused excessive railroad property damage. This number represents about 20% of the total equipment-related derailments [1]. Carter and green's [2] investigation indicates that cracked or broken plate consistently contributes to nearly one quarter of the causes of failure. Also, cracked or broken rims constitutes about 20% of the reported wheel failures.

Figure 1 shows the nomenclature of a wheel. There are wide variety of wheels with different cross-sections and material properties. Wheels are classified into 5 categories, class U, L, A, B and C. Class U has no heat treatment, while class L, A, B, and C have varying degrees of heat treatment [3]. The factors influencing these varieties are manufacturing process, the intended application and the desired service life. The first factor, the manufacturing process, divides the wheel into two main categories, casting which is used in manufacturing of parabolic plate wheels, and forging which is used in making straight plate wheels.

The second factor relates to the type and

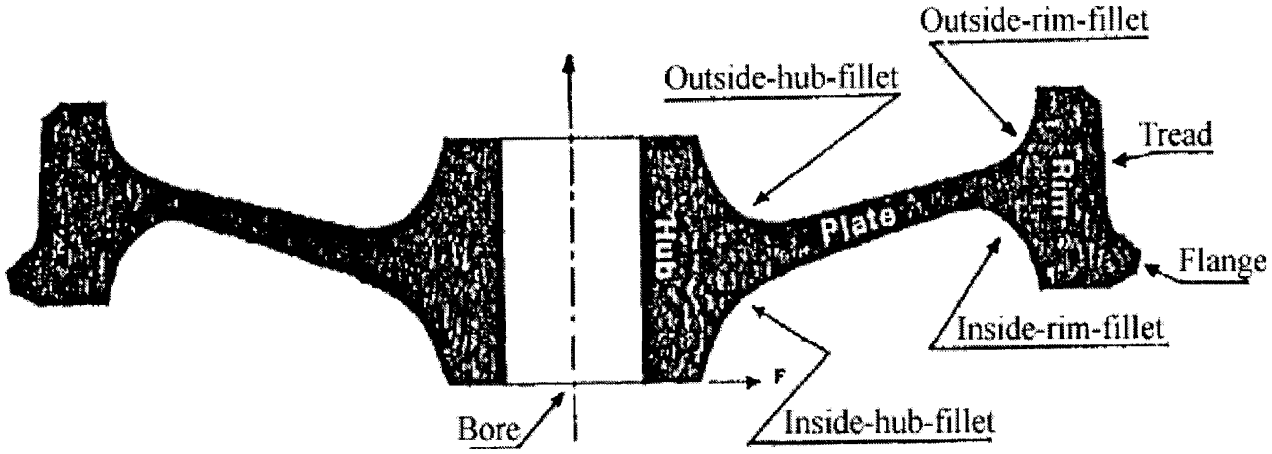

Figure 1. Structure of the Wheel.

severity of application. As one expects, a higher load would require large diameter to keep the rail contact stress within acceptable limits. Thus, the nominal diameters of wheels range from 0.71 to 1.06 meters, corresponding to load ranging from 9.6 kN to 15.2 kN.

The third influencing factor is the desired life. About 85% of the wheels in service are designed for single tread life which is called one-wear wheel. Wheels with thicker rims are designed as either two-wear or multiple-wear wheels. The specifications for minimum rim thickness of one-wear, two-wear and multiple-wear wheels are 3.17, 5.08 and 6.35 cm, respectively.

Besides being an integral part of the train motion, railway wheels are required to perform two main functions in railroad service. The first function is to support the weight of the vehicle, and the other is to provide a brake drum, as shown in Figure 2. So during its service life, a wheel encounters different types of wear and tear such as shelling, spalling, thermal cracking, overheating, etc.

Shelling is caused by fatigue failure of tread due to repeated over-stressing by heavy wheel loads. Spalling develops form service conditions such as wheel slipping, skidding, or sliding.

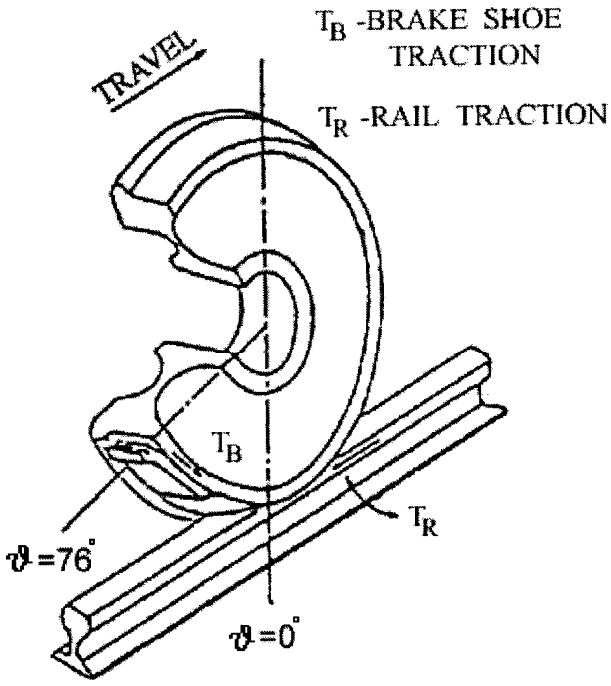

Figure 2. Coordinate (ϑ) system illustrating the location of the wheel-brake shoe (ϑ = 76 deg.) and wheel-rail (ϑ = 0 deg.) planes.

Thermal cracks are caused by intense brake heating. The non-thermal stresses experienced in wheels during service result primarily from the following conditions.

i) Vertical loads due to equipment and car load are applied cyclically along the wheel tread, and may be accelerated by dynamic effects due to

track deviation and operating conditions.
ii) Lateral loads applied against the front of the flange as a result of curve negotiation, hunting, etc.

Carter and Green [2] have reported that for 91.5 cm wheel with 266.4 kN vertical load, the highest stresses are occurring in radial direction. Their values were obtained to be 21.36 MPa at inside-rim-fillet, and 26.87 MPa at outside-hub-fillet. Stresses due to drag braking have been experienced to have crossed the yield limit in some cases.

Novak and Stone [4] have analyzed a 36 inch straight plate wheel under vertical and lateral loads for 55 seconds drag braking. It is observed that as rim thickness decreases, stresses in the rim-plate-fillet and hub-plate-fillet tend to increase.

Rusin et al. [5] have analyzed a 33 inch straight plate wheel and proposed a new design, which is similar to parabolic plate wheel. Up to 30% reduction in thermal stresses is observed in the new design at the fillet regions where the Von Mises stresses are high. However, slight increments of these regions are found to be under mechanical loading. In another study, Rusin et al. [6] have used finite element method for designing a 32 inch curved plate wheel. Their results indicate that the curved beam is less susceptible to the crack problem as well as to high cycle fatigue.

Wetenkamp and Kipp [7] have performed experimental and theoretical analyses on 33 inch parabolic plate wheel. A three dimensional finite element model has been developed. For an 88.8 kN vertical load, the maximum Von Mises stress is observed to be 25 MPa at the outside-hub-fillet which is well bellow the yield limit.

Sakamoto et al. [8] have experimented with a wheel testing machine and have examined the effects of wheel skidding and tread braking on thread shelling of railroad wheels. Their results show that the reversing shear and the maximum shear stress are the main cause of failure.

Woodbury et al. [9] have investigated the effects of mechanical stresses in sub-critically quenched rail car axles. They show that the service loads and maintenance operation do not cause any significant changes in axial compressive mechanical stresses. However, surface defects from machining and decarburization significantly affected measurement of mechanical stresses.

All the above-mentioned studies have examined wheel stresses using elastic analysis. Johnson et al. [10] have performed plastic analysis on 36 inch one-wear, two-wear and worn straight plate wheels, under severe drag brake conditions. High compressive radial mechanical stresses are observed in plate region, but nothing is mentioned about tangential stresses that are tensile in the critical fillet regions as is observed in the present study.

The purpose of the present work is to study the behavior of elasto-plastic and mechanical stresses due to severe drag braking. Also, the intention is to reduce tensile mechanical stresses in regions of stress concentration by modifying the wheel profile, without significantly changing the wheel weight, and load-bearing capacity. Since a large number of wheel manufacturers are producing straight plate wheels, an attempt is made here to reduce stress concentration in a straight plate wheel by only modifying the fillet profiles.

Stress Analysis The irregular shape of wheel makes it impossible to obtain a closed form solution of any comprehensive analytical model

of it. Numerical methods are therefore used to obtain approximate solutions. Since the geometry of the wheel involves many curved boundaries, finite element method is used in the present investigation. Constant strain triangular elements are used based upon its simplicity and its ability to closely model curved contours of the wheel.

Axi-symmetric finite element formulation is obtained by minimization of potential energy:

$$P=\int_V(\{\varepsilon\}^T[D]\{\varepsilon\}/2-\{\varepsilon\}^T([D]\{\varepsilon_h\}+\{\sigma_o\}))dV$$

$$\left.\begin{matrix}\\ \\ \\ \end{matrix}\right\} \int_S \{F_s\}\{d\}ds+\{P\}\{d\} \qquad (1)$$

For an axi-symmetric body, the strain expression is:

$$\{\varepsilon\} = [B]\{d\} \qquad (2)$$

where $\{d\} = \begin{Bmatrix} u_i \\ v_i \\ u_j \\ v_j \\ u_k \\ v_k \end{Bmatrix}$ and

$$[B]=\frac{1}{2A}\begin{bmatrix} 0 & c_i & 0 & c_j & 0 & c_k \\ b_i & 0 & b_j & 0 & b_k & 0 \\ \frac{a_i}{r}+b_i+\frac{c_i}{r}z & 0 & \frac{a_i}{r}+b_j+\frac{c_j}{r}z & 0 & \frac{a_k}{r}+b_k+\frac{c_k}{r}z & 0 \\ c_i & b_i & c_j & b_j & c_k & b_k \end{bmatrix}$$

With a_i, b_i, and c_i coefficients are give as:

$a_i = r_j z_k - r_k z_j$

$a_i = r_k z_i - r_i z_k$

$a_k = r_i z_j - r_j z_i$

$b_i = z_j - z_k$

$b_j = z_k - z_i$

$b_k = z_i - z_j$

$c_i = r_k - r_j$

$c_i = r_i - r_k$

$c_i = r_j - r_i$

Stress strain relationship for an axisymmetric body is given by:

$$\{\sigma\} = [D](\{\varepsilon\} - \{\varepsilon_o\}) \qquad (3)$$

where

$$\{\varepsilon_h\}=\begin{Bmatrix} \varepsilon_{zh} \\ \varepsilon_{rh} \\ \varepsilon_{qh} \\ \varepsilon_{rzh} \end{Bmatrix} = \begin{Bmatrix} \alpha DT \\ \alpha DT \\ \alpha DT \\ 0 \end{Bmatrix}$$

$$[D] = \frac{E}{(1+\nu)(1-2\nu)}\begin{bmatrix} 1-\nu & \nu & \nu & 0 \\ \nu & 1-\nu & \nu & 0 \\ \nu & \nu & 1-\nu & 0 \\ 0 & 0 & 0 & \frac{1-2\nu}{2} \end{bmatrix}$$

The minimization process gives us:

$$\int_V [B]^T[D][B]dV \{d\} = \int [N^T]\{Fs\}ds + \int_V [B]^T[D]\{\varepsilon_T\}dV - \int_V [B]^T\{\sigma_o\}dV + \{P\} \qquad (4)$$

Equation 3 for an element can be written as:

$$[K]\{d\} = \{F\} \qquad (5)$$

The total elasto-plastic strain increment, $d\varepsilon_{ij}$, is the sum of elastic strain, $d\varepsilon^e_{ij}$, and plastic strain, $d\varepsilon^p_{ij}$. The plastic strain increment is based on the generally accepted hypothesis, that:

$$d\varepsilon^p_{ij} = \lambda \frac{\partial Y}{\partial \sigma_{ij}} \qquad (6)$$

where λ is a proportionality constant and Y is the yield criterion. Yielding can occur only if the stress $\{\sigma\}$ satisfy the general yield criterion:

$$Y(\{\sigma\},k) = 0 \qquad (7)$$

where k is a work-hardening parameter. The plastic stress-strain relationship is based on Levy-Mises criteria, that is:

$$de^p_{ij} = \frac{3}{2}\frac{\tilde{A}e}{se}\,s^{\AA}_{ij} \qquad (8)$$

where $s^{\AA}_{ij} = s_{ij} - \frac{(s_z + s_r + s_q)}{3}\,d_{ij}$

$$e = \frac{\sqrt{2}}{3}\left[(e_z - e_r)^2 + (e_r - e_q)^2 + (e_q - e_z)^2 + 6g^2_{zr} + 6g^2_{rq} + 6g^2_{qz}\right]^{1/2}$$

The term s_e/de is the variable plastic modulus, $H^{\AA}$.

The total elastic-plastic stress-strain relationship, also known as Prandtl-Reuss equation:

$$de_{ij} = \frac{1+v}{E}\,ds_{ij} - \frac{v}{E}\,ds_{kk}\,d_{ij} + \frac{3}{2}\frac{de}{s}\,s^{\AA}_{ij}$$

$$= [D]^{-1}\,ds_{ij} + l\,\frac{\tilde{A}Y}{\tilde{A}s_{ij}} \qquad (9)$$

When plastic yield is occurring the stresses are on the yield surface, given by Equation 13. Differentiating Equation 6 and using the Prandtl-Reuss equation, we get:

$$\left\{\frac{\tilde{A}Y}{\tilde{A}\{s\}}\right\}^T d\{s\} + H^{\AA} l = 0 \qquad (10)$$

where

$$\frac{\tilde{A}Y}{\tilde{A}\{s\}} = \left\{\frac{\tilde{A}Y}{\tilde{A}s_z}\;\frac{\tilde{A}Y}{\tilde{A}s_r}\;\frac{\tilde{A}Y}{\tilde{A}s_q}\;\frac{\tilde{A}Y}{\tilde{A}s_{rz}}\right\}^T$$

$$= \frac{3}{s}\left\{\frac{s^{\AA}_z}{2}\;\frac{s^{\AA}_r}{2}\;\frac{s^{\AA}_q}{2}\;t_{rz}\right\}^T$$

where primes (Å) are deviatoric stresses, e.g.

$$s_{ij}\AA = s_{ij} - \frac{s_z + s_r + s_q}{3}\,d_{ij}$$

In this study, the stress-strain curve is assumed to be bilinear, in that the value of HÅ is constant for the whole plastic region.

RESULTS AND DISCUSSIONS

The displacement of wheel profile results in compressive radial and tangential stresses in the inside-rim-fillet and tensile radial and tangential stresses in the outside-hub-fillet regions. This is illustrated from the elastic stress distribution in a wheel after brake application of 20 hp for 30 minutes, as shown in Figure 3. High Von Miss stresses are observed in inside-rim-fillet and outside-hub-fillet regions, causing initiation of yielding in those regions, which is evident from the extent of yielded region for 20 hp brake application for 60 minutes, shown in Figure 4, where only outside-hub-fillet and inside-rim-fillet regions have yielded. The triangle represent the yielded regions. Application of higher horsepower brakes cause increase in the yielded region. Since the temperature in the rim section is very high, and wheel material properties are greatly affected by high temperatures, a considerable part of the rim section is found to have yielded due to brake application of 30 hp and 40 hp for 60 minutes, which is shown in Figure 4.

Elastic-plastic stresses are obtained for the wheel subjected to yielding, from 20 hp, 30 hp and 40 hp of brake application for 60 minutes, shown in Figure 5. High compressive tangential stresses and tensile radial stresses are found in the rim section. Slight reduction is observed in both radial and tangential stresses in this region for 40 hp case, Figures 5(a) , as compared to 30 hp, Figures 5(b) , due to larger yielded region of the former. In outside-hub-fillet and inside-rim-fillet regions, high tensile radial and tangential stresses are found.

Mechanical stresses, shown in Figure 6(a) and (b), are obtained for the wheel by subtracting the elastic stresses. Tensile tangential stresses and compressive radial stresses are found in the rim and inside-rim-fillet regions, while tensile radial and compressive tangential stresses are found in

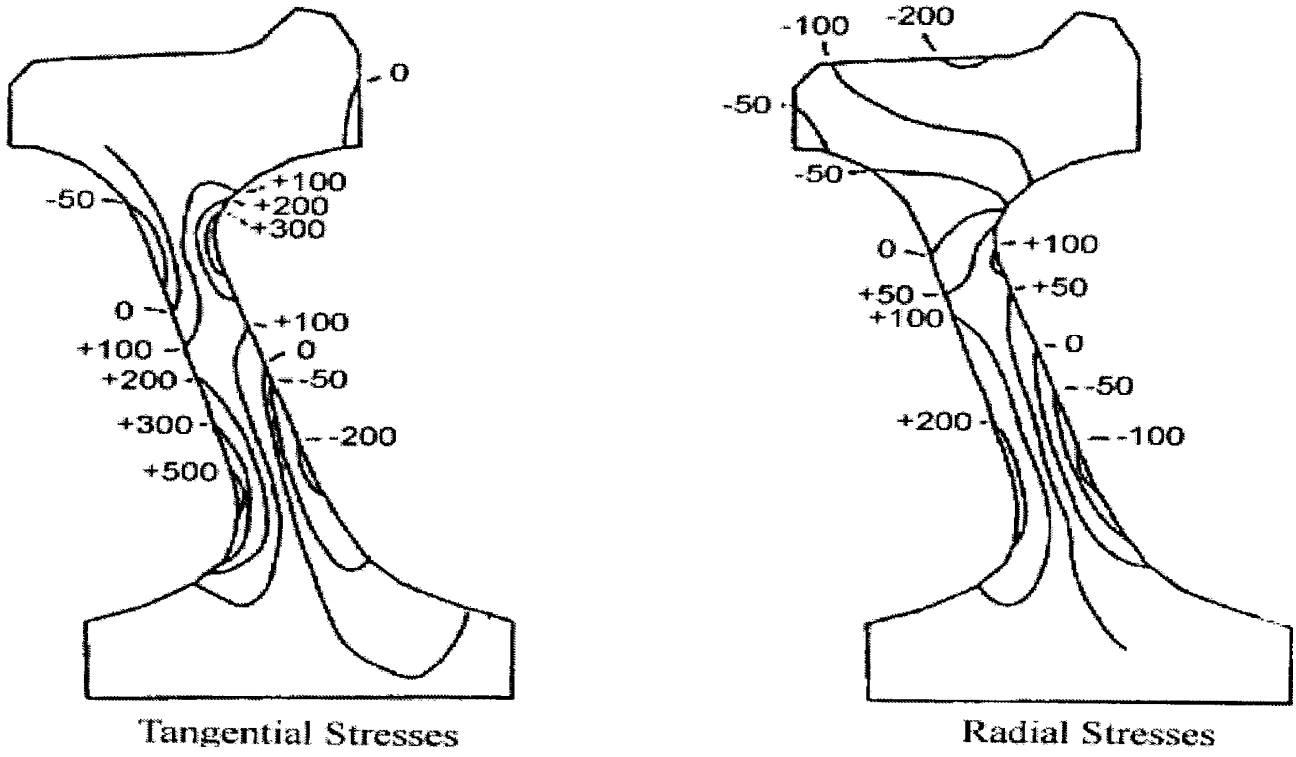

Figure 3. Elastic stress distribution in wheel after 20 hp brake application for 30 minutes. All values in MPa.

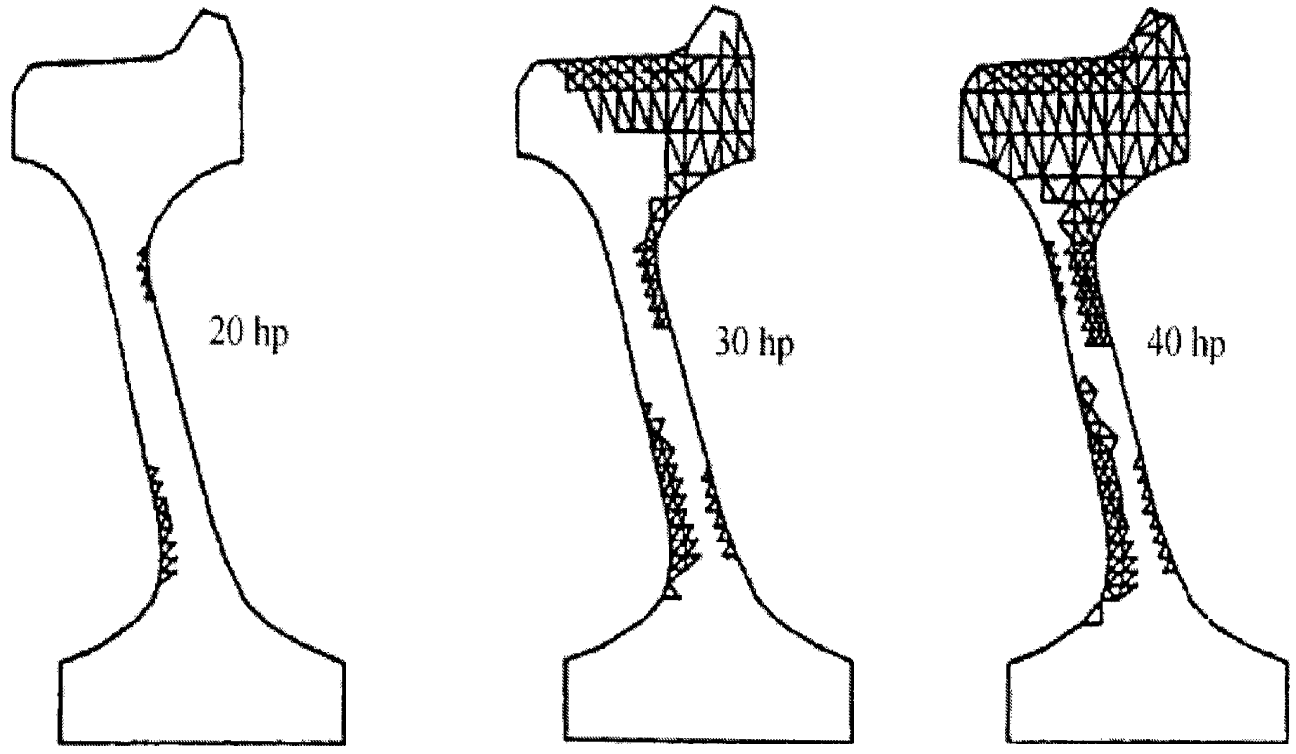

Figure 4. Extension of yield region in wheel after drag brake application for 60 minutes.

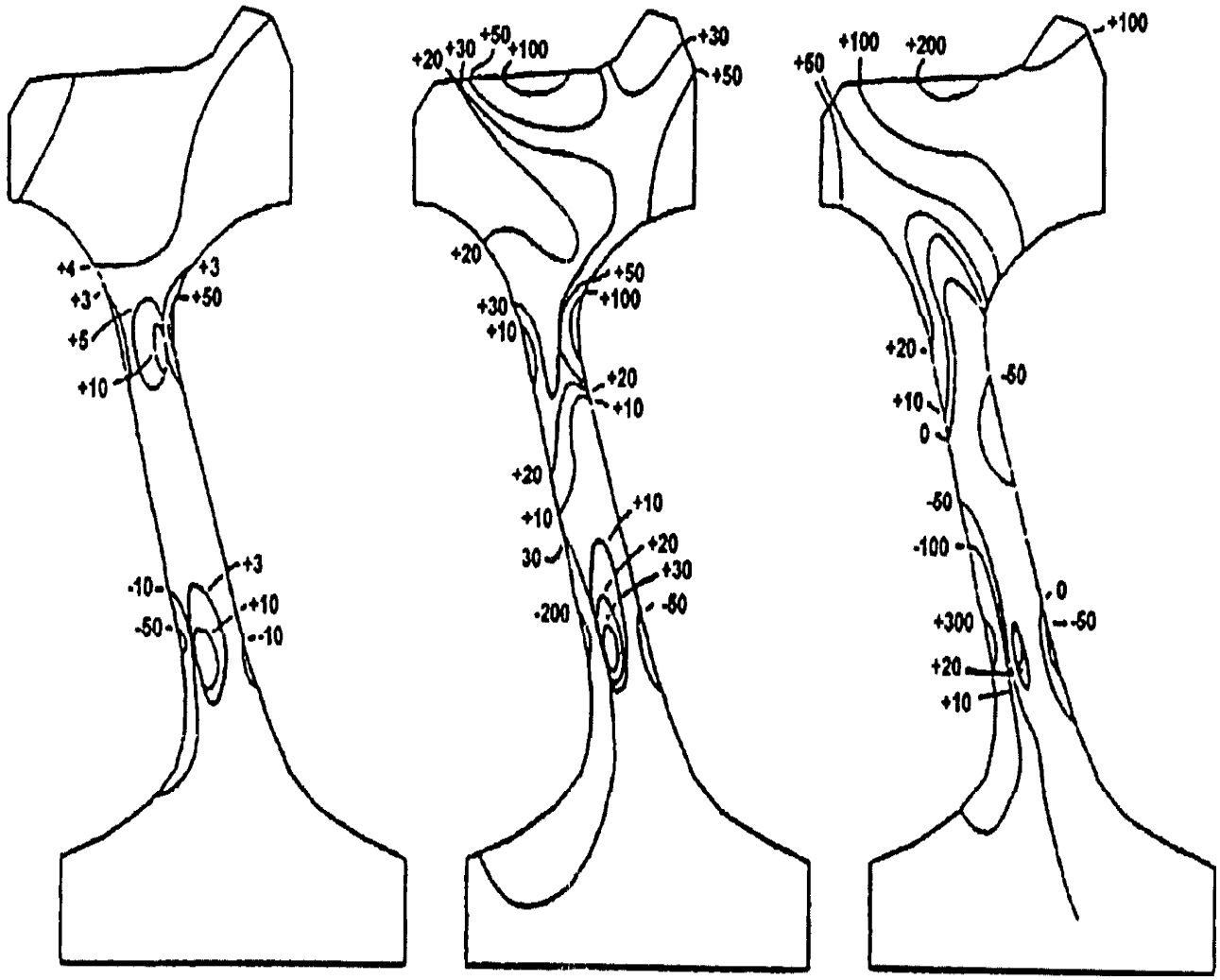

Figure 5(a). Elasto-plastic radial stress distribution in wheel after 20 hp, 30 hp, 40 hp brake application for 60 minutes. All values are in MPa.

outside-hub-fillet regions. Fillet areas are found to be the regions of high stress concentration.

Tensile radial stresses are very important factors in fatigue failure. Their presence contributes towards reduction of fatigue life, since they act as the mean stress. Fatigue strength is seriously reduced by the presence of stress concentration. So it is imperative that the tensile mechanical stresses around the areas of stress concentration should be reduced.

Reduction in tensile mechanical stresses by improving the profile of wheel fillets will improve the fatigue life of the wheel. For this reason, three new designs are tested. Improvement in profile is done in the inside-rim-fillet and outside-hub-fillet regions, since they are high stress areas. The three new designs are presented in Figure 7, along with the old design. For design # 1 and # 2 there is no significant change in weight, while design #3 where z and r are coordinates, and a, b, c, and d are constants given in Table 1. The three new designs are analyzed elasto-plastically and mechanical stresses are obtained for each of them. Brake energy of 30 hp for 60 minutes is used for this purpose.

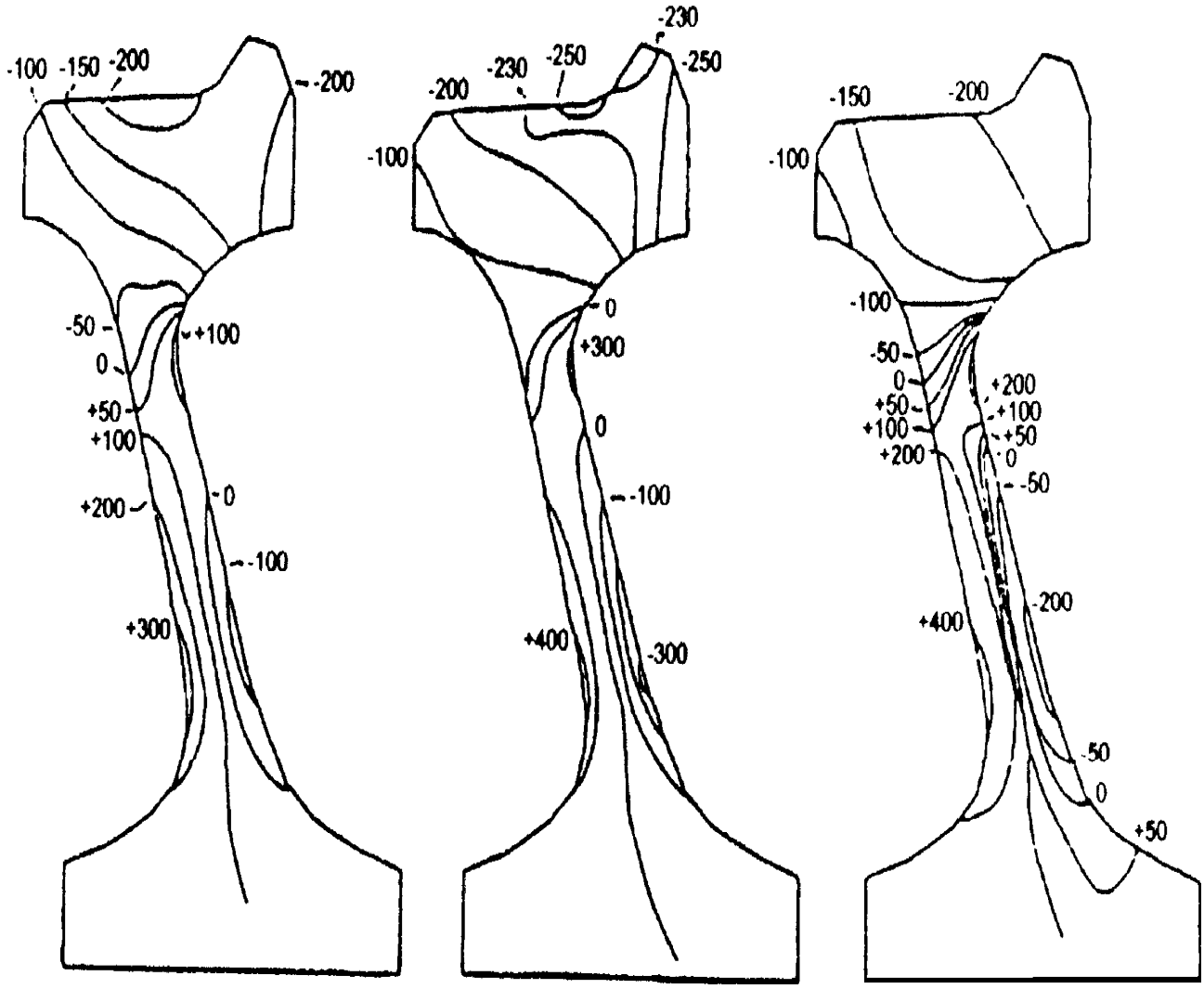

Figure 5(b). Elasto-plastic tangential stress distribution in wheel after 20 hp, 30 hp, 40 hp brake application for 60 minutes. All values are in MPa.

has 4% increase in weight. The fillet profiles can be represented by a polynomial:

$$z = ar^3 + br^2 + cr + d \quad (11)$$

Obviously the design with reduction in high tensile mechanical stresses is a better one, but reduction in one region may cause an increase in tensile mechanical stresses in some other regions. For that reason comparison between the mechanical stresses of the four different designs is done using a ``penalty'' function, by assigning weights to fifteen different locations on the wheel as shown in Figure 8 and explained in Table 2. These weights are given in accordance with the relative sensitivity of the location and the stresses. For example, the locations with high tensile stresses are given high weights while the locations with high compressive stresses are given low weights. W_t and W_r are the weights assigned to tangential and radial stress at a location respectively. More than one location of comparison are used around yielded region, while for the regions which are not yielded only one location is used. For example outside-hub-fillet region has

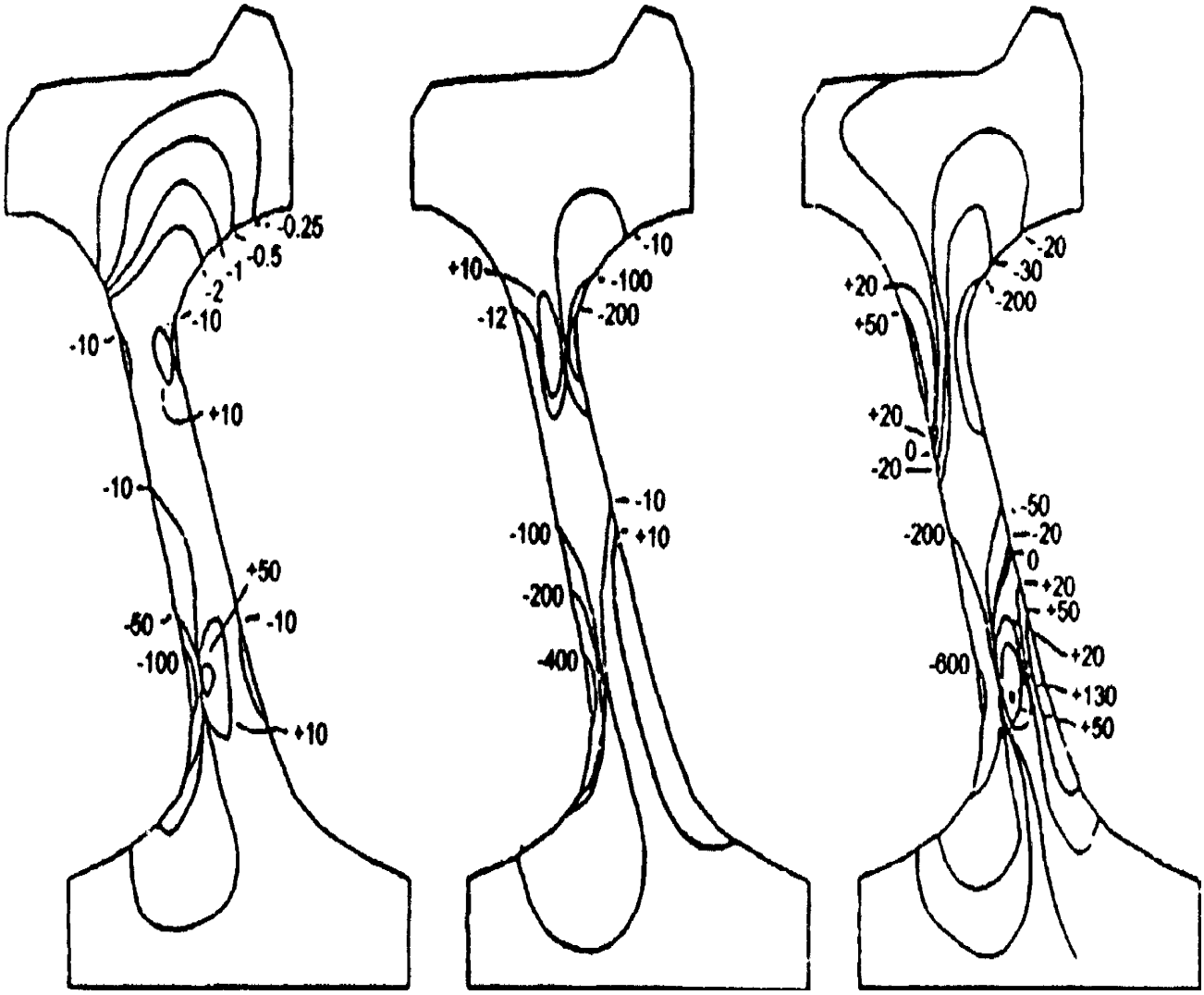

Figure 6(a). Mechanical radial stress distribution in wheel after 20 hp, 30 hp, 40 hp brake application for 60 minutes. All values are in MPa.

locations 1, 2, and 3 which fall within the yielded region in that area. Similarly locations 7, 8 and 9 fall within the yielded region in rim section, while location 12 represents the unyielded region of the rim. The penalty function used is:

$$C_f = \sum_{i=1}^{15} \left[(W_t)_i \, (Ds_q)_i + (W_r)_i \, (Ds_r)_i \right] \qquad (12)$$

where Ds for a particular location is the difference in stress of the new design being compared and the stress of the old design for the same location. The design with smallest number (greatest negative number) is the best design under these consideration.

The mechanical stresses obtained in all four designs at the fifteen locations are presented in Figures 8 to 11. These stresses along with their proper weights are used in the penalty function, Equation 12, to find the penalty of the new designs. For design # 1 the cost is -653, for design #2 the cost is -955 and for design #3 it is -548. Since for design # 2 the penalty is the least, -955, it is the best of the three designs.

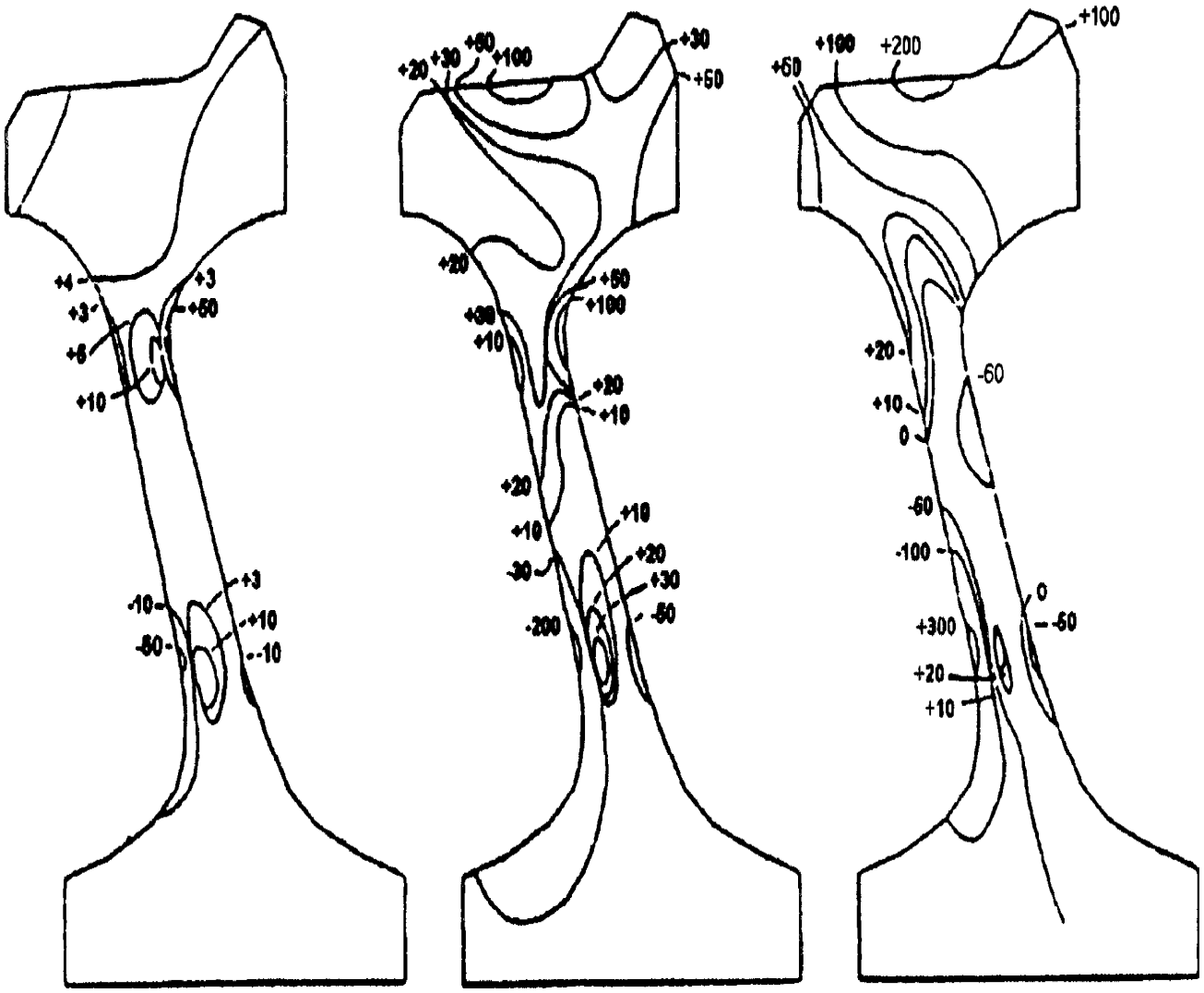

Figure 6(b). Mechanical tangential stress distribution in wheel after 20 hp, 30 hp, 40 hp brake application for 60 minutes. All values are in MPa.

Considering the cases physically, in the rim region, locations 7, 8 and 9, design has a slight increase in tensile tangential stresses, as compared to design # 1, but in the areas of stress concentration, locations 6 and 11, there is a reduction in tensile stresses in design # 2. Similarly between designs # 2 and # 3, around critical region of inside-rim-fillet the tensile stresses are lower in #2 than in #3. Moreover, as shown in Table 3, the old design and design # 1, undergo more deformation under thermal loads than do designs #2 and #3, as is observed by the changes in tread taper, ($b_{å} - b_{d}$), and plate inclination, ($y_{å} - y_{d}$), angles. Also, designs # 2 and # 3 have about the same deformation, which further supports that design # 2 with considerable reduction in mechanical stresses and smaller wheel deflection is the best of the four designs.

CONCLUSIONS

Railway wheel failure has been a major concern

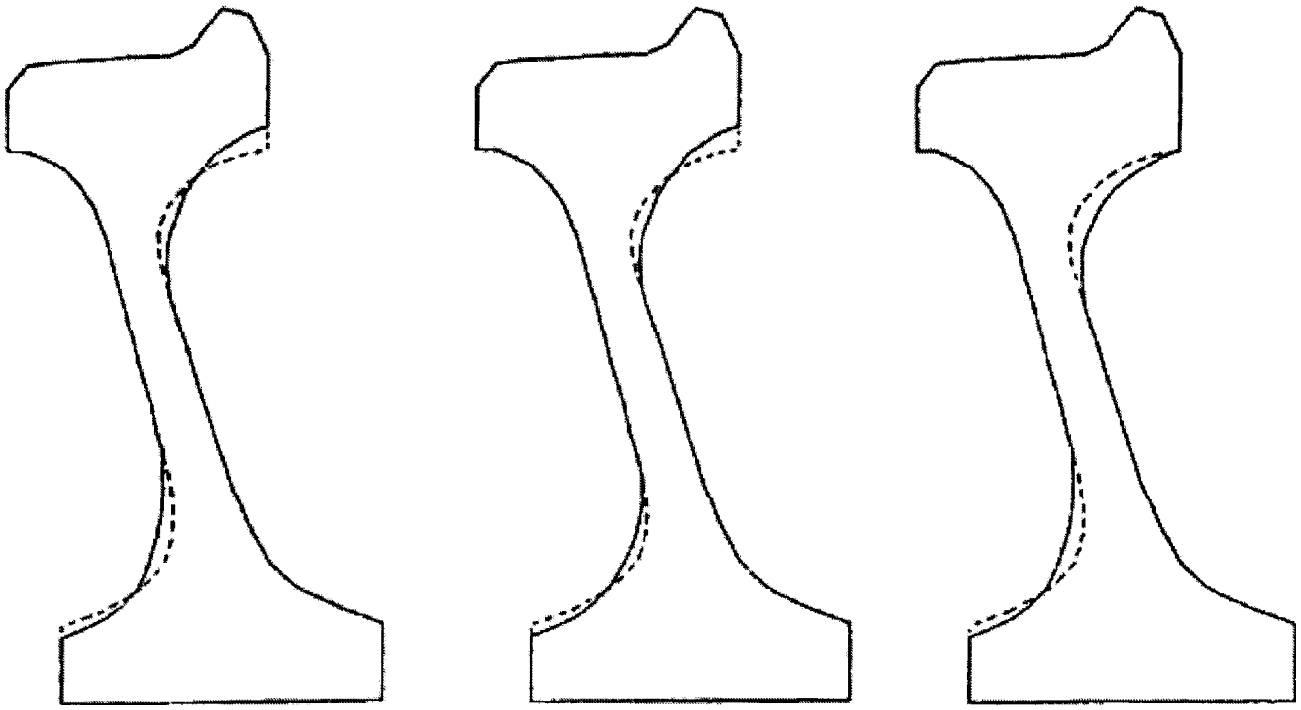

Figure 7. The mew designs considered for the wheel profile.
(--- for the original design and __ for the new designs).

TABLE 1. Constants of Equation 11 for Representation of Fillet Profiles.

Inside-Rim-Fillet					
Design	a	b	c	d	Fillet radius range, cm
old	+0.0346	-3.722	+133.12	-1573.82	41.9<r<33.53
#1	+0.0073	-0.7297	+24.15	-254.82	43.18<r<33.53
#2	+0.0073	-0.7297	24.15	-254.82	43.18<r>33.53
#3	+0.013	+1.335	45.5	-506.4	41.9<r>33.53

Outside-Hub-Fillet					
Design	a	b	c	d	Fillet radius range, cm
old	-0.02212	+1.5704	-36.88	+298.27	16.5<r<25.9
#1	+0.1246	+0.8997	-21.543	+182.95	15.9<r<25.9
#2	-0.0168	+1.1589	-26.64	+215.77	15.9<r>25.9
#3	-0.0168	+1.1589	-26.64	+215.77	15.9<r>25.9

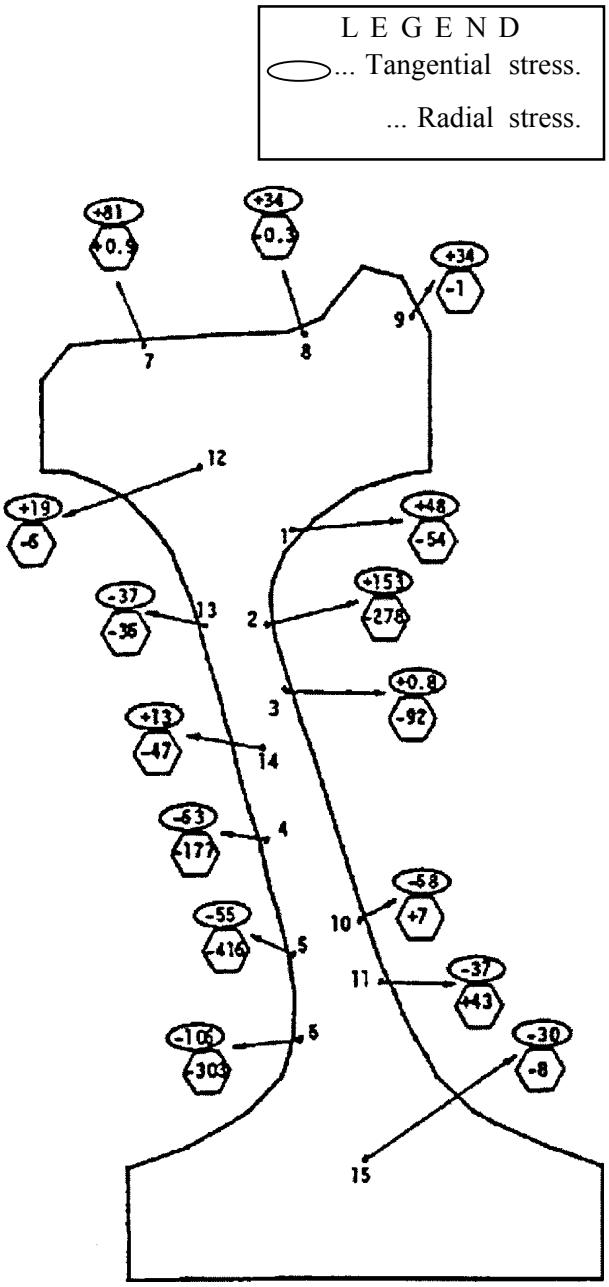

Figure 8. Mechanical stress distribution at the fifteen locations of the old design. All stresses are in MPa.

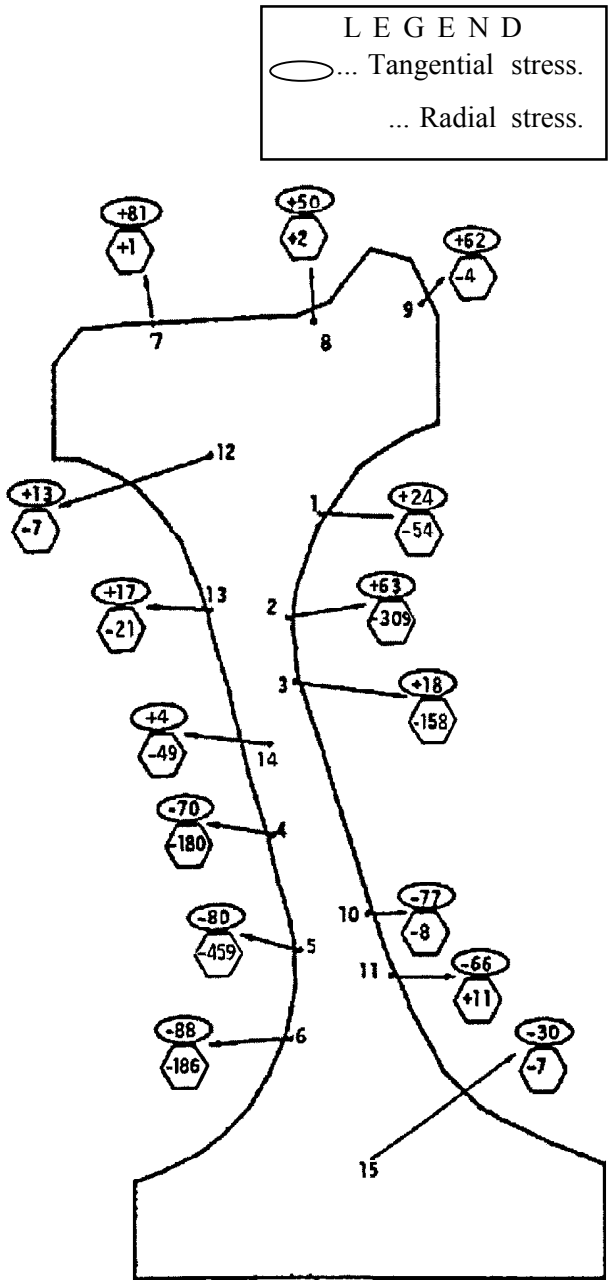

Figure 9. Mechanical stress distribution at the fifteen locations of the new design #1. All stresses are in MPa.

to engineers for the few decades due to increasing trend in heavy trian loads and high speed requirements. These wheels not only help in traveling and support car load, but also act as break drums. They experience a great deal of stresses during service life. Under server drag braking, the heat from brake energy travel deep inside the wheel and reduce the tread taper and plate inclination. The stresses caused by thermal gradient are extremely high.

TABLE 2. Weights assigned to the radial and tangential stresses of the fifteen locations considered for stress comparison.

Location	Weights	Remarks
1,2,3	$W_t = 7$ $W_r = 1$	High tangential tensile mechanical stresses. In practice cracks are found in this region. High radial compressive stresses. A little reduction in compressive stresses will not contribute in failure.
4, 5, 6	$W_t = 2$ $W_r = 1$	Compressive tangential stresses. High compressive radial stresses.
7, 8, 9	$W_t = 4$ $W_r = 0.5$	Tensile tangential stresses. Increase in that will move the situation towards fatigue failure. Very small radial stresses.
10, 11	$W_t = 2$ $W_r = 3$	Compressive stresses. Tensile radial stresses.
12	$W_t = 1$ $W_r = 1$	Small tensile stresses. Compressive radial stresses.
13	$W_t = 2$ $W_r = 2$	Small compressive stresses. Small compressive radial stresses.
14	$W_t = 1$ $W_r = 1$	Small tensile tangential stresses. Compressive radial stresses.
15	$W_t = 1$ $W_r = 1$	Compressive tangential stresses. Compressive radial stresses.

TABLE 3. Changes in Tread Taper Angle and Plate Inclination Angle for Different Designs.

Design	Change in angles (deg.)	
	$(b_o - b_d)$	$(y_o - y_d)$
Old	1.50	2.01
#1	1.05	1.67
#2	0.43	0.78
#3	0.40	0.74

Due to the irregular shape of the wheel the finite element technique is used for stress analysis. This technique is found to be very useful elasto-plastic stress analysis. The wheel is divided into more than 430 elements, and the brake energy is simulated as spread load on a 70 mm wide strip on tread surface. Mechanical stresses are obtained for the wheel. Tensile tangential and radial mechanical stresses are found in inside-rim-fillet and outside-hub-fillet

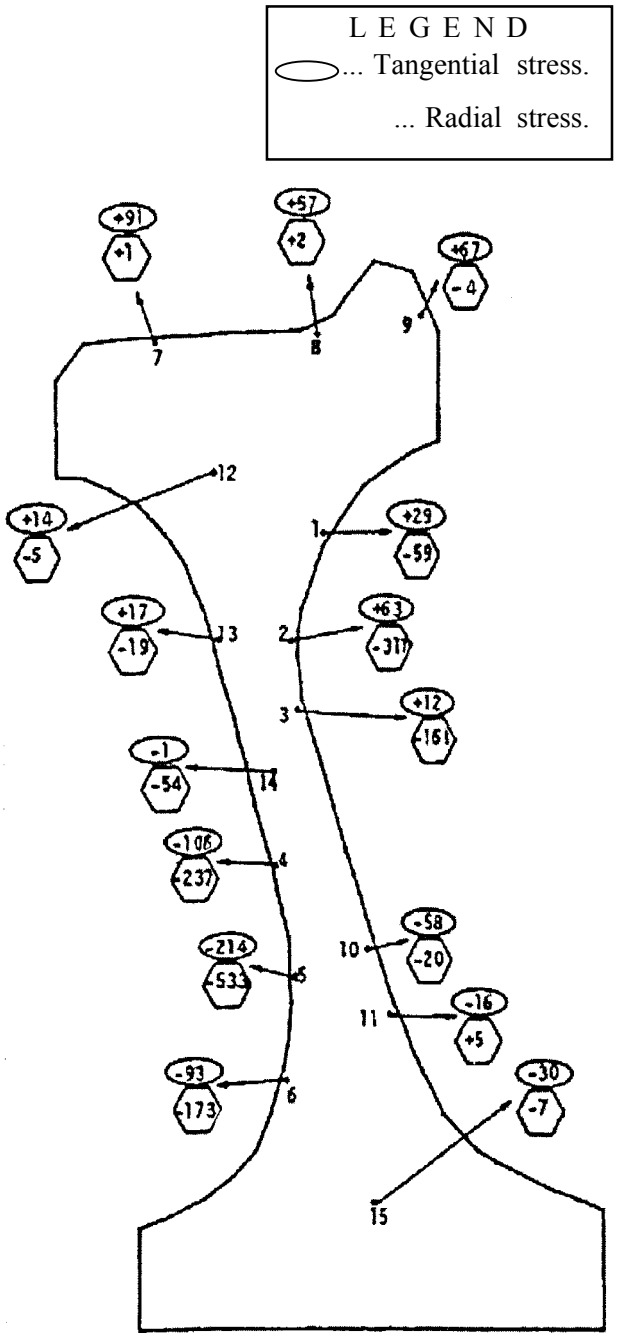

Figure 10. Mechanical stress distribution at the fifteen locations of the new design #2. All stresses are in MPa.

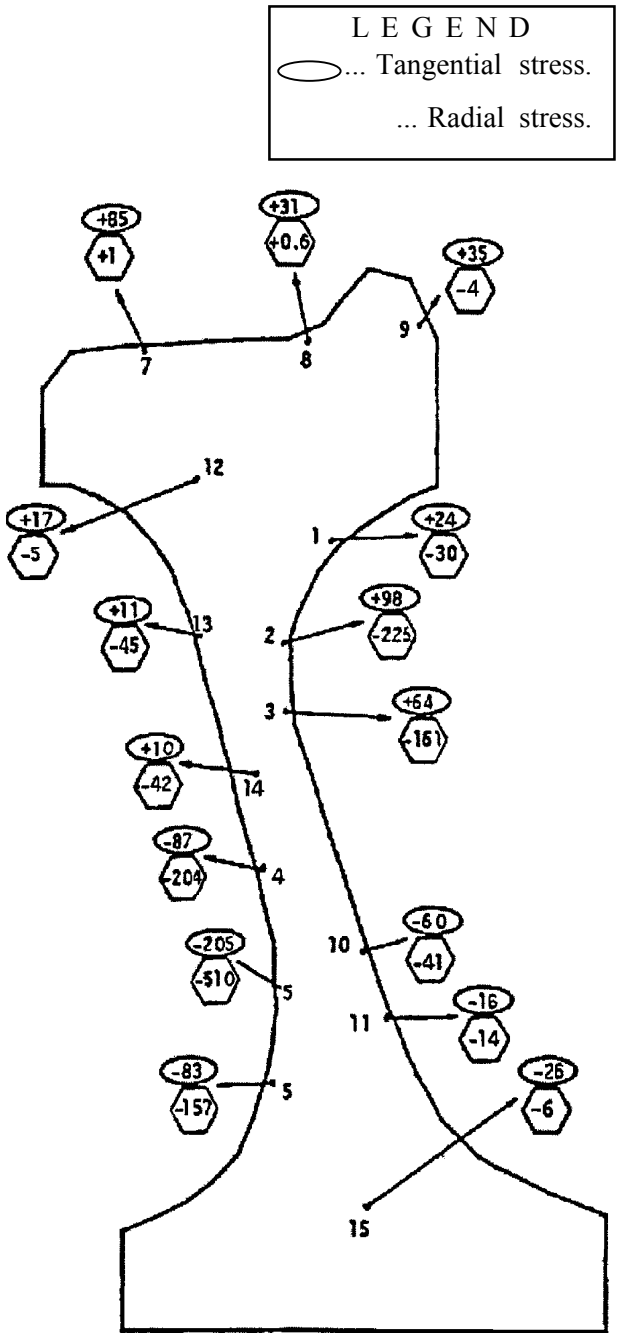

Figure 11. Mechanical stress distribution at the fifteen locations of the new design #3. All stresses are in MPa.

regions respectively. These tensile mechanical stresses are critical in the fatigue of a wheel, especially since they are in region of high stress concentration.

Attempt is made to reduce these tensile mechanical stresses by modifying fillet profiles. Three new designs with modifications in fillet profiles are tested. Care is taken to avoid

significant changes in the wheel weight in the new designs. Mechanical stresses are obtained for the new designs and are compared with mechanical stresses in the old design. A penalty function is used for the comparison of stresses.The possibility of using penalty function, as a means of comparison of stress variation with design change, is demonstrated in this paper. Design #2 is found to be the best of the three new designs, with a considerable reduction in the maximum tensile mechanical stresses as compared to the old design.

The attempt in this study shows that a slight variation in the fillet profiles has a significant effect on the stress distribution in the wheel. Since many of the wheel manufacturers make straight plate wheels, and the manufacturing processes for both straight plate and parabolic plate wheels are considerably different, it is advisable to produce a better wheel applying the findings of research in this regard.

NOMENCLATURE

A	=	Area of triangular element, m^2.
[B]	=	Matrix relating stress and strain.
[C]	=	Capacitance matrix.
[D]	=	Elasticity matrix.
$[D]_{ep}$	=	Elasto-plastic matrix.
E	=	Modulus of elasticity, MPa.
{F}	=	Force vector.
$\{F_s\}$	=	Surface forces.
$H^{\AA}$	=	Plastic modulus, Mpa.
i, j, k	=	Nodes of a triangle.
[K]	=	Stiffenss matrix.
[N]	=	Shape function.
{P}	=	Vector contaning nodal forces.
r	=	Radial direction.
u	=	Displacements in radial direction.
v	=	Displacements in axial direction.
V	=	Volume, m^3.
W_r	=	Weight assigned to radial stress.
W_t	=	Weight assigned to tangential stress.
z	=	Axial direction.
b_0	=	Original tread taper angle = $3.06^{\AA}$.
b_d	=	Deflected taper angle, deg. y.
g	=	Shear strain.
q	=	Tangential direction.
d_{ij}	=	Kronecker delta.
{d}	=	Displacements.
e	=	Normal strain.
e_e	=	Equivalent strain.
$\{e_h\}$	=	Thermal strain.
r	=	Density of the material, kg/m^3.
s	=	Normal stress, MPa.
s_e	=	Equivalent stress, MPa.
s_o	=	initial stress, MPa.
`s	=	Yield stress, MPa.
t	=	Shear stress, MPa.
y_o	=	Original tread taper angle = $18.43^{\AA}$.
y_d	=	Deflected taper angle, deg.

REFERENCES

1. Leadly, G. L., ``An Overview of current Efforts To Detect And Prevent Steel Wheel Failures'', ***Natl. Bur. Stand. Spec. Publ.***, No. 436, pp 261-288, (1975).
2. Carter, C. S. and Green, R. G., ``Fracture Resistance of Railroad Wheels", ***U. S. Dept. of Transportation***, Report No. FRA-ORD & D-75-12, Sept. (1974).
3. Literature Supplied by Hawker Sidley Canada Ltd., ``Railway Wheel Data'', Canadian Steel Wheel Division, ``Montereal, Canada.
4. Novak, G. E. and Stone, D. H., ``CyclicDistortion And Stresses In 36 in. Wheels Under Comined Service Loads", ASME Paper #75-WA/RT-S.
5. Rusin, T. M., Kleeshulte, D. G. and Coughlin, J.M., ``Application of The Finite Element Method In The Development of Improved Railroad Car Wheel Design," ***ASME Paper #78-WA/RT-5***.
6. Rusin, T.M., Coughlin, J.M. and Damergis, G. "Curved Plate Wheel Design For A Commuter Railroad's Reverse Dish 32" Car Wheel," ***ASME Railroad Transportation***, Vol. 12, pp. 79-85, (1996).
7. Wetenkamp, H. R. and Kipp, R.M., ``Thermal Damage

And Rail Load Stresses In A 33 in. Railroad Car Wheel,'' ***Trans. ASME, J. of Eng. For Industry***, pp. 363-369, (Aug. 1978).

8. Sakamoto, H., Hirakawa, K., Toyama, K. and Nishimura, S. "Simulation Test on Tread Shelling of Railroad wheel", ***ASME International Mech. Eng. Congress & Exposition Proc.***, pp. 73-78, (1996).
9. Woodbury, C. A., Pearson, J. B., Downs, W. E. and Brandimarte, G. "Effects of Service on Residual Stresses in Subcritically Quenched Rail Car Axles", ***J. RTD, Tans. ASME***, Vol. 12, pp. 97-104, (1996L.
10. Young K. S., Johnson, M. R. and Welch, R. E. ``Analysis of Thermal Stresses and Residual Stress Changes In Railroad Wheels Caused By Severe Drag Braking'', ***Trans. ASME, J. of Eng. For Industry***, pp 18-23, (Feb. 1977).
11. Zienkiewicz, O. C., Valliapan, S. and King, I. P., ``Elasto - Plastic Solution of Engineering Problems, Initial Stress, Finite Element Approach'', ***Int. J. Num. Methods In Eng.***, Vol. 1, pp 75-100, (1969).